ACS APPLIED MATERIALS & INTERFACES

Research Article

www.acsami.org

Flame-Retardant Electrical Conductive Nanopolymers Based on Bisphenol F Epoxy Resin Reinforced with Nano Polyanilines

Xi Zhang,[†,‡] Qingliang He,[†] Hongbo Gu,[†] Henry A. Colorado,[§] Suying Wei,*[,‡] and Zhanhu Guo*[,†]

[†]Integrated Composites Laboratory (ICL) Dan F. Smith Department of Chemical Engineering, Lamar University, Beaumont, Texas 77710, United States

[‡]Department of Chemistry and Biochemistry, Lamar University, Beaumont, Texas 77710, United States

[§]Department of Mechanical and Aerospace Engineering, University of California Los Angeles, Los Angeles, California 90095, United States

Supporting Information

ABSTRACT: Both fibril and spherical polyaniline (PANI) nanostructures have successfully served as nanofillers for obtaining epoxy resin polymer nanocomposites (PNCs). The effects of nanofiller morphology and loading level on the mechanical properties, rheological behaviors, thermal stability, flame retardancy, electrical conductivity, and dielectric properties were systematically studied. The introduction of the PANI nanofillers was found to reduce the heat-release rate and to increase the char residue of epoxy resin. A reduced viscosity was observed in both types of PANI−epoxy resin liquid nanosuspension samples at lower loadings (1.0 wt % for PANI nanospheres; 1.0 and 3.0 wt % for PANI nanofibers), the viscosity was increased with further increases in the PANI loading for both morphologies. The dynamic storage and loss modulii were studied, together with the glass-transition temperature (T_g) being obtained from the peak of tan δ. The critical PANI nanofiller loading for the modulus and T_g was different, i.e., 1.0 wt % for the nanofibers and 5.0 wt % for the nanospheres. The percolation thresholds of the PANI nanostructures were identified with the dynamic mechanical property and electrical conductivity, and, because of the higher aspect ratio, nanofibers reached the percolation threshold at a lower loading (3.0 wt %) than the PANI nanospheres (5.0 wt %). The PANI nanofillers could increase the electrical conductivity, and, at the same loading, the epoxy nanocomposites with the PANI nanofibers showed lower volume resistivity than the nanocomposites with the PANI nanospheres, which were discussed with the contact resistance and percolation threshold. The tensile test indicated an improved tensile strength of the epoxy matrix with the introduction of the PANI nanospheres at a lower loading (1.0 wt %). Compared with pure epoxy, the elasticity modulus was increased for all the PNC samples. Moreover, further studies on the fracture surface revealed an enhanced toughness. Finally, the real permittivity was observed to increase with increasing the PANI loading, and the enhanced permittivity was analyzed by the interfacial polarization.

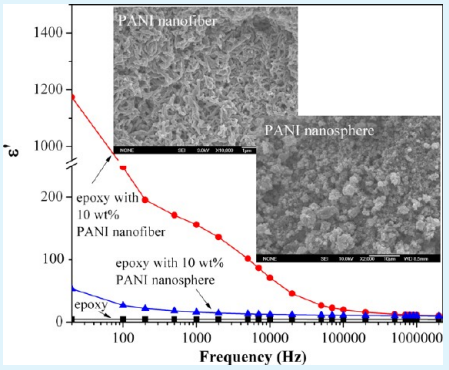

KEYWORDS: *epoxy resin nanocomposites, filler−polymer interaction, viscoelastic property, tensile properties, nanospheres and nanofibers*

1. INTRODUCTION

The development of conductive or semiconductive polymer nanocomposites (PNCs) from insulating polymers has attracted more interest, because of the introduced unique physicochemical properties to the otherwise inert hosting polymers, such as thermal stability,[1−3] magnetic,[4−6] optical,[7−9] and dielectric properties.[10−13] Epoxy as one of the most important engineered polymers has drawn attention because of its wide applications, including structural materials, tissue substitutes,[14] anticorrosion coatings,[15] and flame-retardant additives.[16] However, the industrial deployments of epoxy resin are largely limited by the static electricity problem. Different types of conductive fillers such as carbon nanofibers (CNFs),[17,18] carbon nanotubes (CNTs),[19] iron nanoparticles,[20] copper and nickel powders,[21] and electrically conductive glass fibers with a conductive coating[22] have been attempted to increase its electrical conductivity (σ). However, easy oxidation and high density of the metal particles on one side cause a reduced conductivity and heavy weight of the final products,[23] which will definitely challenge the required device and structure miniaturization.[24,25] On the other side, the easy agglomeration of CNTs and CNFs is always deleterious to the mechanical properties of the final finishings, and the required surface treatments for their better dispersion increase the nanocomposite cost.[26,27] Polyaniline (PANI), among all the conjugated polymers, is more attractive, because of its

Received: November 3, 2012
Accepted: December 28, 2012
Published: December 28, 2012

controllable doping levels.[28−33] However, PANI synthesized in the classical approaches from aniline, oxidant, and small molecule acid[34] has very poor solubility in common solvents such as ethanol, methanol, and acetone.[35] PANI nanostructures with large interfacial areas between PANI and their surroundings[36] can have an improved dispersibility in the hosting matrixes.

In addition to the increased conductivity,[37] the epoxy-PANI composites have other certain unique properties.[38,39] For instance, a high dielectric constant is observed in the PANI−epoxy composites fabricated by the in situ polymerization method.[40] Oligomeric PANI (o-PANI) shows a very low threshold value.[41] PANI can even act as a curing agent for epoxy resin with covalent bondings formed between the amine groups of PANI and epoxy resin, and the heat of curing increases as the PANI loading increases.[42] Although the electrical conductivity of the epoxy-PANI nanocomposites has been achieved by increasing the loading[43] or decreasing the size[44] of PANI, the morphology effect has not been studied yet. In addition, a comprehensive study on the rheological behaviors, flame retardancy, and dynamic mechanical properties of these epoxy nanocomposites filled with soft polymer nanostructures has been rarely reported.

Generally, two types of nanoparticles are applied to enhance the flame retardancy of the polymer matrix. One is the inorganic nanoparticles including alumina trihydrate,[45] layered double hydroxides (LDHs),[46] clay,[47] and montmorillonite (MMT).[48] However, the flame retardancy of the nanocomposites with inorganic nanoparticles largely depends on their dispersion quality.[45] Because of the poor compatibility between organic and inorganic materials, additional surface modification[49] or compatibilization[50] is normally deployed to achieve good dispersion of silicate nanoparticles in the polymer matrix. The other type of additive is organic nanoparticles, such as phosphorus-based[51−53] and nitrogen-based flame retardants, including melamine and its derivatives.[54] For flame retardants with phosphorus functional groups, during the decomposition process, the phosphorus-rich layer can be formed on the surface of residues and be separated from heat source.[55] However, the phosphorus-based flame retardants demand that the matrix contain oxygen or nitrogen atoms to promote char formation, which prevent further combustion. Otherwise, coadditives are required to act as charring agents.[53] During the research of nanocomposite flame retardancy, the nitrogen-based flame retardants have attracted more and more interest, because of their efficient performance that can function in all the burning stages. These nitrogen-based flame retardants can lead to endothermic reactions,[54] which will release ammonia gases at higher temperature to dilute oxygen and combustible gases.[53] In addition, the nitrogen-based flame retardants can enhance the char formation. For instance, the melamine cyanurate (MCA), which was used to improve the flame retardancy of polyamide 6 (PA6) nanocomposites, can promote the generation of carbonaceous char in the condensed phase and further slow the degradation of the matrix.[48] PANI, which contains the nitrogen compounds in the side chain and aromatic ring, has potential applications as flame retardants.[56] However, limited research about its flame retardancy property in epoxy matrix has been reported.

In this paper, two different laboratory-synthesized PANI nanostructures—nanofibers and nanospheres—were applied as conductive nanofillers in epoxy resin to enhance the electrical conductivity and increase the fire retardancy performance. The PNCs with different loading level and morphology of PANI nanofillers were prepared. The rheological behaviors of the uncured samples (liquid phase) were studied including steady-state viscosity and complex viscosity, together with the storage and loss modulii. And, for all the cured samples (solid phase), the thermal stability was studied by thermogravimetric analysis (TGA) test and the flame retardancy performance was evaluated by microscale combustion calorimetry, considering the heat release capacity (HR capacity), peak heat release rate (pHRR), total heat release, and the char residue. The thermomechanical properties, including storage and loss modulii, and glass-transition temperature were evaluated together with the tensile strength and Young's modulus. The effects of PANI loading and morphology on the electrical conductivity and dielectric property also were systematically studied. The observed enhanced dielectric properties were interpreted by the interfacial polarization.

2. EXPERIMENTAL METHODS AND CHARACTERIZATION

2.1. Materials. The epoxy resin Epon 862 (bisphenol F epoxy) and EpiCure W curing agent were purchased from the Miller−Stephenson Chemical Company, Inc. The molecular structures of these chemicals are shown in Scheme S1 in the Supporting Information. Aniline (C_6H_7N), ammonium persulfate (APS, 98 wt %, $(NH_4)_2S_2O_8$), and *p*-toluene sulfonic acid (PTSA, 98.5 wt %, $C_7H_8O_3S$) were all purchased from Sigma−Aldrich. Chloroform ($CHCl_3$) was purchased from Fisher Scientific. All of the chemicals were used as received without any further treatment.

2.2. Preparation of PANI Nanofibers (NFs). PANI NFs were prepared by an interfacial polymerization method with an aniline:APS:PTSA ratio of 8:2:25. Briefly, aniline (3.2 mmol) was dissolved in chloroform (10 mL) as Solution 1, and Solution 2 was prepared by dissolving APS (0.8 mmol) in 1.0 M PTSA aqueous solution (10 mL). Then, Solution 2 was added into Solution 1 quickly and maintained still for 2 h of polymerization at room temperature. The product was vacuum-filtered and washed with ethanol and deionized water to remove any possible oligomers, excess acid, and extra organic solvent. The obtained powders were dried completely at 50 °C.

2.3. Preparation of PANI Nanospheres (NSs). The molar ratio used in this method was aniline:APS:PTSA = 6:3:5. For Solution 1, PTSA (60 mmol) and APS (36 mmol) were dissolved in deionized water (400 mL) in a beaker and ultrasonicated in an ice water bath for 1 h. Solution 2 was aniline (72 mmol) dissolved in deionized water (100 mL). Solution 2 then was added into Solution 1 and the mixture was sonicated for an additional hour in an ice water bath for polymerization. Finally, the product was vacuum-filtered and washed with ethanol and deionized water to remove any possible oligomers, excess acid, and organic solvent. The obtained powders were dried at 50 °C.

2.4. Preparation of PANI−Epoxy Nanocomposites. Epoxy resin suspensions with 1.0, 3.0, 5.0, and 10.0 wt % of PANI NFs and NSs were prepared. First, PANI nanostructures were immersed in epoxy resin (the total weight of epoxy resin and curing agent was fixed to 40.0 g, and the PANI loading in epoxy resin was controlled by varying the weight of PANI nanostructures) without any disturbance overnight so that the resin could wet the nanostructures completely. The mixture was then mechanically stirred (Heidolph, Model RZR 2041) at a speed of 600 rpm for 1 h at room temperature. The Epicure

W curing agent was added into the above suspension with a weight ratio of monomer/curing agent of 100/26.5, as recommended by the company, and the solution was stirred at high speed (600 rpm) for another hour at room temperature. In order to remove bubbles in the solution and prevent the settlement of PANI nanofillers during the curing process, low-speed (200 rpm) mechanical stirring was conducted at 70 °C for 3−4 h in a water bath. Finally, the solution was poured into silicon rubber molds and cured at 120 °C for 5 h and then cooled naturally to room temperature.

2.5. Rheological Behaviors of Liquid Epoxy Resin Nanosuspensions. The rheological behaviors of the epoxy resin nanocomposite suspensions, were investigated with a rheometer (AR 2000ex, TA Instrumental Company) at shear rates ranging from 0.1 rad/s to 1200 rad/s at 25 °C (the samples are a mixture of only epoxy monomers and nanofillers). A series of measurements were performed in a cone-and-plate geometry with a diameter of 40 mm and a truncation of 64 μm. Dynamic rheological measurements were also performed with a sweeping frequency range between 0.1 s^{-1} and 1000 s^{-1} at a low strain (1%), which was justified to be within the linear viscoelastic (LVE) range for these materials. The LVE range was determined by the strain-storage modulus (G') curve within the strain range from 0.01 to 100 at a frequency of 1 rad/s. Specimens placed between the cone and plate were allowed to equilibrate for ∼2 min prior to each frequency sweeping.

2.6. Fourier Transform Infrared Spectroscopy (FT-IR). The FT-IR spectroscopy (Bruker, Inc., Model Vector 22, coupled with an ATR accessory) was used to characterize the surface functionality of pure PANI nanostructures, pure epoxy resin, and PANI NFs treated with epoxy resin in the range of 500−4000 cm^{-1} at a resolution of 4 cm^{-1}.

2.7. Thermal Characterization of PANI−Epoxy Nanocomposites. The thermal stability of the cured PANI−epoxy PNCs was studied via thermogravimetric analysis (TGA) (TA Instruments, Model Q-500). All the samples were heated from 30 °C to 700 °C with a nitrogen flow rate of 60 mL/min and a heating rate of 10 °C/min. The samples were tested in air condition with the same flow rate and heating rate to compare the thermal stability of PNCs under different conditions. Differential scanning calorimetry (DSC) (TA Instruments, Model Q2000) measurements were implemented under a nitrogen flow rate of ∼20 mL/min at a heating rate of 10 °C/min from 0 °C to 400 °C.

2.8. Flame Retardancy Characterization of Cured Epoxy Nanocomposites. The flame retardancy performance was evaluated by using a microscale combustion calorimeter (MCC) (Model MCC-2, Govmark, Farmingdale, NY), according to American Society for Testing and Materials (ASTM D7309, Method A). The sample (∼3 mg) was heated to a specified temperature using a linear heating rate (1 °C/s) in a stream of nitrogen at a flow rate of 80 mL/min. The thermal degradation products of the sample in nitrogen were mixed with a 20 mL/min stream of oxygen prior to entering the 900 °C combustion furnace. The reported MCC parameters were the averages of three measurements.

2.9. Mechanical Characterization of Cured Epoxy Nanocomposites. Dynamic mechanical analysis (DMA) measurements were carried out in the torsion rectangular mode using a Model AR 2000ex system (TA Instrumental Company) with a strain of 0.05%, a constant frequency of 1 Hz, and a heating rate of 2 °C/min in the temperature range of 30−200 °C. The sample dimensions were 12 mm × 3 mm × 40 mm.

Tensile tests were carried out following ASTM methods (Standard D 412-98a, 2002) in a unidirectional tensile testing machine (ADMET tensile strength testing system). The parameters (displacement and load) were controlled by a digital controller (MTEST Quattro) with MTESTQuattro Materials Testing Software. The samples were prepared as described for the nanocomposite fabrication in silicon rubber molds, which were designed according to the standard ASTM requirement. A crosshead speed of 1.00 mm/min was used and the strain (mm/mm) was calculated by dividing the crosshead displacement by the original gauge length.

2.10. Morphological Characterizations of PANI−Epoxy Nanocomposites and PANI Nanostructures. After the tensile test, the broken samples of the PANI−epoxy nanocomposites were collected. The morphology of the fracture surfaces and the morphology of PANI nanostructures were characterized with a field-emission scanning electron microscope (SEM) (JEOL, Model JSM-6700F). Before testing, the samples were first coated with a thin gold layer.

2.11. Resistivity and Permittivity Measurements of Cured PANI−Epoxy Nanocomposites. The volume resistivity was determined by measuring the DC resistance along the disc samples with diameters ∼60 mm. An Agilent Model 4339B high-resistance meter was used to measure the samples. This equipment allows resistance measurement up to 10^{16} Ω. The reported values represent the mean value of eight measurements with a deviation of <10%.

The dielectric permittivity was measured by a LCR meter (Agilent, Model E 4980A) equipped with a dielectric test fixture (Agilent, Model 16451B) in the frequency range of 20 Hz−2 MHz. The samples used for the tests were disk pellets with a diameter of 40 mm and the average thickness was ∼2 mm. A piece of rectangular standard Teflon sample with a permittivity of 2.1−2.4 was used for calibration before each test.

3. RESULTS AND DISCUSSION

3.1. PANI Nanofibers and Nanospheres. Two different types of PANI nanostructures were synthesized by two different methods and used as conductive nanofillers to enhance the properties of epoxy. Interfacial polymerization method yielded PANI nanofibers, while PANI nanospheres were obtained by using ultrasonication (see Figure 2). Compared with PANI nanospheres with an average diameter of 370 nm, PANI nanofibers have an average diameter of 142.7 nm and length of 1.00 μm (Figure 2). In addition, because of the higher aspect ratio, the PANI nanofibers exhibit larger specific surface area than the PANI nanospheres.[57] However, the PANI nanospheres have a better thermal stability than nanofibers in nitrogen condition (see Figure 1A). For both PANI nanofillers, a slight weight loss stage can be observed from room temperature to 150 °C, which is attributed to the release of moisture and organic solvent residue entangled in the polymer chains.[58] The flame retardancy behaviors of these two PANI nanofillers were also studied and the heat release capacity (HR capacity), peak heat release rate (pHRR), total heat release, and char residue are summarized in Table 1. The PANI nanospheres are observed to have a higher decomposition temperature (285.69 °C) than the PANI nanofibers (260.45 °C) (Figure 1B), which is consistent with the TGA result. However, the total heat release of the PANI nanofibers were lower than those of the PANI nanospheres. Although the onset

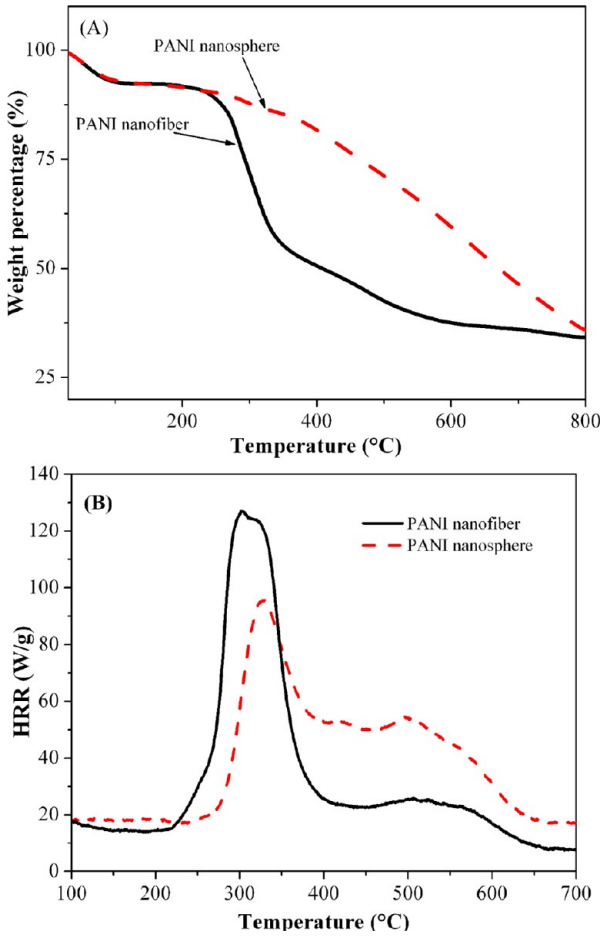

Figure 1. (A) TGA curves and (B) the HRR−temperature curves of PANI nanofibers and PANI nanospheres.

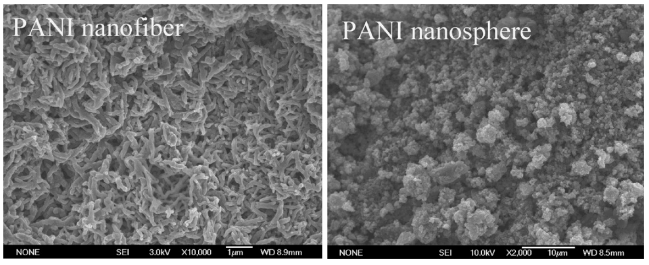

Figure 2. SEM microstructures of PANI nanofibers and nanospheres.

decomposition temperature of the PANI nanofibers is lower, the heat release process concentrates on a narrow temperature range (~260−400 °C), after reaching the pHRR, the HRR value decreases sharply with increasing temperature. However, for the PANI nanospheres, the heat release process takes place over a wide temperature range (~285−650 °C), compared with the PANI nanofibers, the HRR value of the nanospheres maintains a large number in the temperature range of 400−600 °C. This phenomenon can also be observed in the TGA thermal stability study (Figure 1A). The PANI nanofibers exhibit a sharp weight loss; however, the PANI nanospheres decompose slowly over a wide temperature range. (The differential thermogravimetry (DTG) result is shown in Figure S2 in the Supporting Information.) Thus, the total heat release of the PANI nanofibers is lower than those of the PANI nanospheres.

Table 1. Heat Release (HR) Capacity, Peak Heat Release Rate (pHRR), Total Heat Release and Char Residue for the Cured Pure Epoxy, PANI Nanofibers, PANI Nanospheres, and PNCs with PANI Nanofibers and Nanospheres

	HR capacity (J/(g K))	peak HRR (W/g)	total HR (kJ/g)	char residue (%)
cured pure epoxy	491	664.3	28	12
PANI nanofibers	107	113.4	11.6	40
PANI nanospheres	73	77.69	11.9	51
PNCs with 1.0 wt % PANI nanofibers	381	518.8	27.0	11
PNCs with 3.0 wt % PANI nanofibers	344	465.5	26.7	12
PNCs with 5.0 wt % PANI nanofibers	318	429.2	26.0	13
PNCs with 10.0 wt % PANI nanofibers	243	325.6	23.7	21
PNCs with 10.0 wt % PANI nanospheres	285	381	24.9	18

3.2. Rheological Behaviors of PANI-Epoxy Resin Nanosuspensions. The rheological behaviors were tested for pure epoxy resin and its nanosuspensions containing PANI nanofillers. The increase of shear stress is almost linear with increasing the shear rate. (The detailed results of shear stress vs shear rate are shown in Figure S1 in the Supporting Information.) The viscosity is observed to decrease as the shear rate increases (see Figures 3A and 3B). However, not all

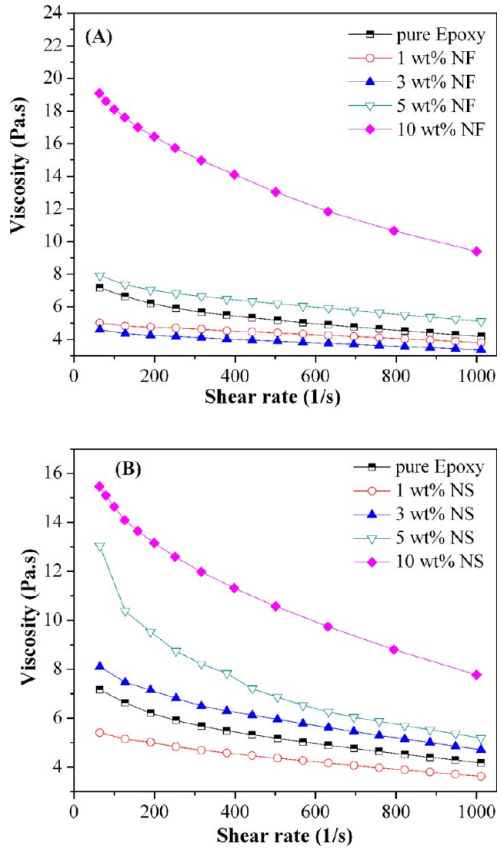

Figure 3. Viscosity versus shear rate of (A) pure epoxy resin and its nanosuspensions with different PANI nanofiber (NF) loading, and (B) pure epoxy resin and its nanosuspensions with different PANI nanosphere (NS) loading.

dx.doi.org/10.1021/am302563w | ACS Appl. Mater. Interfaces 2013, 5, 898−910

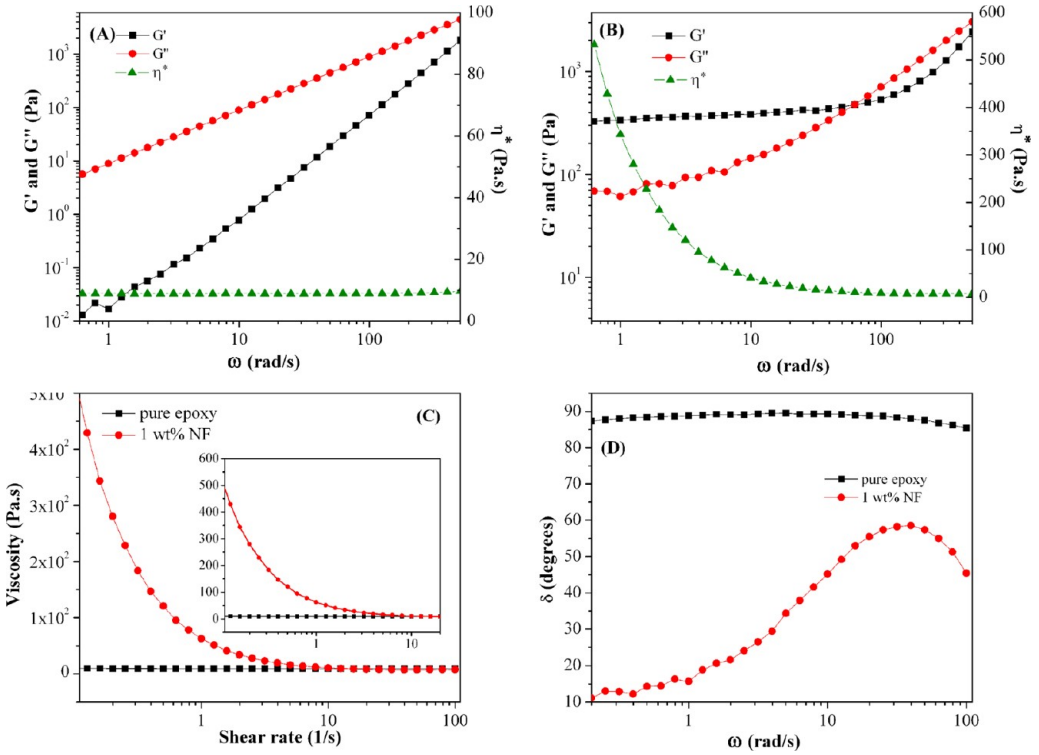

Figure 4. Complex viscosity (η^*), G', and G'' vs ω of (A) pure epoxy resin and (B) epoxy resin nanosuspensions with 1.0 wt % PANI nanofibers; (C) viscosity vs shear rate of pure epoxy resin and epoxy resin nanosuspensions with 1.0 wt % PANI nanofibers (the inset shows the limited shear rate scale from 0 to 20 rad/s); and (D) δ vs frequency of pure epoxy resin and epoxy resin nanosuspensions with 1.0 wt % PANI nanofibers.

of these behaviors can be considered as shear-thinning process (for polymer fluid, the shear force can induce the disentanglement of polymer chains, which will further align along the shear direction[59] to cause a decreased shear viscosity with increasing the shear rate[60]). The identification of shear-thinning process was further studied with the complex viscosity.

Figures 4A and 4B show the storage modulus (G'), loss modulus (G''), and complex viscosity (η^*) of liquid samples of pure epoxy resin and its nanosuspensions with 1.0 wt % PANI nanofibers, respectively. For pure epoxy resin, no crossing point of G' and G'' can be observed in the test range (Figure 4A). The crossing point of the G' and G'' curves can serve as a criteria to identify the switch from viscous liquid to elastic solid.[17] During the frequency sweep test, the angular frequency (ω) was varied from 100 rad/s to 0.1 rad/s. Pure epoxy resin cannot form a solidlike elastic network by itself, and the value of G'' is higher than G'. The gap between these two modulii increased with increasing frequency. However, for epoxy resin nanosuspensions with 1.0 wt % PNAI nanofibers at higher ω, G'' was higher than G', which was the same as pure epoxy resin, the crossing point of G' and G'' is shown at a frequency of ~60 rad/s; with further decreases in ω (lower than 60 rad/s), G' became larger than G'' (Figure 4B). This crossing point represents the fluid property changing from viscous to elastic. Thus, the addition of PANI nanofibers favors the formation of the cross-link among epoxy resin and causes the transition from viscous behavior in the high-frequency range to elastic behavior in the low-frequency range.

The complex viscosity of pure epoxy resin is constant in the entire frequency range (Figure 4A). However, for the epoxy resin nanosuspensions with 1.0 wt % PANI nanofibers, the complex viscosity is decreased as the frequency is increased (Figure 4B). The complex viscosity can be transferred to a steady-state viscosity (viscosity obtained from a ramp-strain experiment[61]) with shear rate, using the Cox–Merz rule (see eq 1):[62]

$$\eta(\dot{\gamma}) = |\eta^*(\omega)|_{\omega=\dot{\gamma}} = \sqrt{\left[\left(\frac{G'}{\omega}\right)^2 + \left(\frac{G''}{\omega}\right)^2\right]}_{\omega=\dot{\gamma}} \quad (1)$$

where $\eta(\dot{\gamma})$ is the steady-state viscosity; $\eta^*(\omega)$ is the complex viscosity; G' and G'' are storage and loss moduli, respectively; ω is the angular frequency; and $\dot{\gamma}$ is the shear rate (when $\omega = \dot{\gamma}$, the value of the complex viscosity is equal to that of the steady-state viscosity). At low shear rate (below 100 s^{-1}), for pure epoxy resin, the steady-state viscosity (transferred from complex viscosity) is constant with increasing the shear rate, which follows Newtonian fluid flow (see Figure 4C). However, for epoxy resin nanosuspensions with PANI nanofillers, the shear viscosity decreases sharply with increasing the shear rate, which is the feature of a pseudo-plastic (shear thinning) fluid. As shown in the steady-state test (Figure 3), at lower loadings of PANI nanofibers (1.0 and 3.0 wt %) and nanospheres (1.0 wt %), with the shear rate increases, the structure of the nanosuspensions would be destroyed and the viscosity decreased to even lower than that of pure epoxy resin. However, with the loading of PANI nanostructures further increased, the interaction between the PANI nanostructures and the epoxy would become stronger, thus, the viscosity of the nanosuspensions is higher than that of pure epoxy.

To further confirm the fluid type, another parameter is introduced by using oscillation test of the liquid samples. The term delta (δ), representing the phase angle between G'' and G', is also obtained as a function of angular frequency. The phase angle of pure epoxy resin is almost 90° (see Figure 4D),

dx.doi.org/10.1021/am302563w | ACS Appl. Mater. Interfaces 2013, 5, 898–910

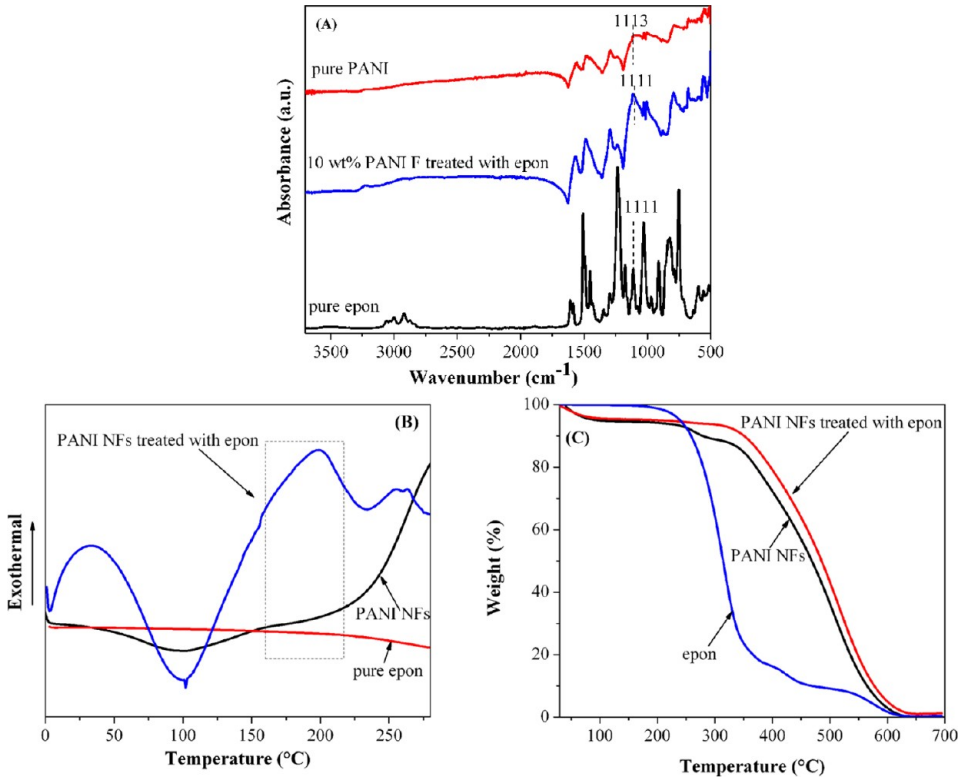

Figure 5. (A) FT-IR spectra, (B) DSC, and (C) TGA curves of pure epoxy resin, pure PANI nanofibers (NFs), and PANI NFs treated with epoxy resin.

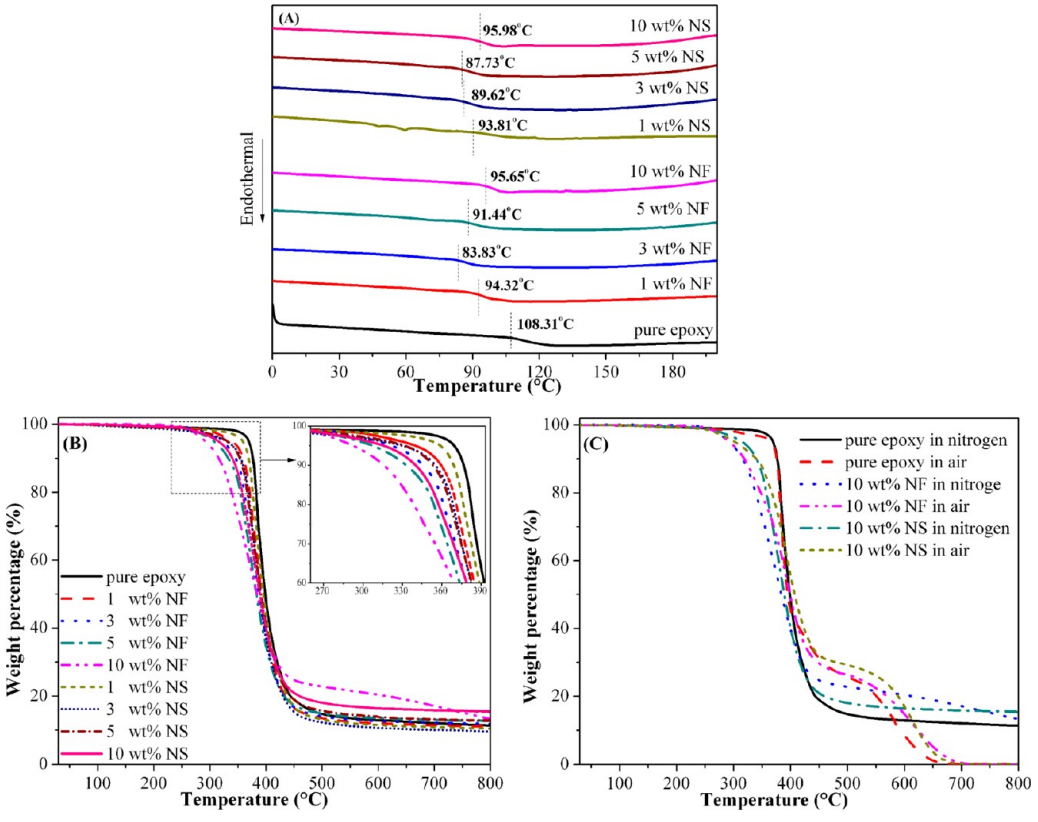

Figure 6. (A) DSC curves of the cured pure epoxy and its PNCs with different loading levels of PANI nanofibers and nanospheres, (B) TGA curves of the cured pure epoxy and its PNCs with different loading levels of PANI nanofibers and nanospheres in nitrogen, and (C) TGA curves of the cured pure epoxy and its PNCs with 10.0 wt % loading of PANI nanofibers and nanospheres in air.

dx.doi.org/10.1021/am302563w | ACS Appl. Mater. Interfaces 2013, 5, 898−910

indicating a Newtonian fluid.[63] Thus, the decreased viscosity in pure epoxy resin sample is not a shear thinning phenomenon; it should be caused by sample splashing under high rotating speed of cone. However, for the epoxy resin nanosuspensions with 1.0 wt % PANI nanofibers, δ is way below 90° (Figure 4D), demonstrating that these nanosuspensions follow shear thinning flow, which is obviously shown in the complex viscosity study (see Figure 4C). Thus, the epoxy resin nanosuspensions with PANI nanofillers belong to a pseudoplastic fluid. Actually, from Figure 4C, the zero-shear viscosity (limiting viscosity at zero shear rate,[64] $\eta_0 = \lim_{\dot{\gamma}\to 0} \eta$) of the epoxy resin nanosuspensions with PANI nanofillers is higher than that of pure epoxy resin, which obeys Newtonian's law; however, the viscosity of the solution decreases (characteristic of pseudoplastic fluid) and becomes even lower than that of pure epoxy resin with increasing shear rate (Figure 4C). All the results of viscosity study indicate that, because of the interaction between the amine groups in the PANI nanofillers and the epoxy resin, PANI nanofillers can promote the epoxy network formation, the interaction between epoxy resin and PANI nanofillers is further explored by FT-IR, DSC, and TGA tests (section 3.3).

3.3. Interactions between Epoxy and PANI Nanofillers. To study the interaction between epoxy resin and PANI nanofillers, epoxy resin nanosuspensions with 10 wt % PANI nanofibers were prepared by following the same procedures without the addition of the Epicure W curing agent. After being heated at 120 °C in an oven for 5 h, the sample was washed with acetone to remove epoxy resin, then the PANI nanofibers (NFs) treated with epoxy resin was obtained and dried in an oven, which were then studied and compared with the pristine PANI NFs. As shown in Figure 5A, after treated with epoxy resin, the peak at 1113 cm^{-1} corresponding to the C−N stretch of quionid ring in PANI[10] shifts to 1111 cm^{-1}, which can be further tracked in the epoxy resin and is related to the C−O vibration.[55,65] The peak shift in the FT-IR test indicates the reaction between amine groups of PANI and epoxy resin. For the DSC test, in Figure 5B, comparing with PANI NFs and pure epoxy resin, an exothermal peak is observed at ∼175 °C for PANI NF sample treated with epoxy, the exothermal peak is associated with the curing process of epoxy resin,[55] demonstrating that, to some extent, the PANI nanofibers can act as a curing agent and initiate the curing process of epoxy, which further proves the interaction between the PANI NFs and epoxy resin. In addition, the thermal stability study (Figure 5C), shows that the onset decomposition temperature is largely increased from 231.62 °C for the PANI NFs to 340.70 °C for the PANI NFs treated with epoxy, which is consistent with the observation that the interaction between the nanofillers and epoxy can postpone the decomposition of the PANI NFs.[42]

3.4. Differential Scanning Calorimetry (DSC) of Cured Epoxy Resin and Its Nanocomposites. For thermosetting systems, gelation, curing, vitrification, and devitrification events can be studied with DSC tests.[66] In general, the former two processes can be observed in uncured samples; however, if the material is not fully cured, an exothermal peak, which represents the curing process, can also be observed for the cured samples. All the samples are observed to be well-cured without any curing peak (see Figure 6A). The existence of nanofillers in the cured epoxy resin is observed to cause a decrease in the glass-transition temperature (T_g) than the cured pure epoxy. The reduced T_g is related to the enlarged free volume arising from the interface between fillers and epoxy resin,[67] which provides more space for polymer chain segments to move, even at a lower temperature. However, when the nanofiller loading is increased to a certain point, the T_g value will increase as the loading of PANI nanofillers increases and the changing point of T_g from decrease to increase occurs at a different loading, i.e., 5.0 wt % for nanofibers and 10.0 wt % for nanospheres. The restrained movement of epoxy chains is due to the formed covalent bondings between epoxy matrix and the amine groups in PANI,[42] which cause an increase in T_g. Thus, the variation of T_g in the PNCs is a competition between two effects, i.e., enlarged free volume and interaction between PANI nanofillers and epoxy matrix. In the PNCs at lower PANI loading level, the free volume effect is dominating, T_g first decreases with increasing the PANI loading. However, when the PANI loading is increased to a certain level, T_g becomes largely dependent on the covalent bonding and increases as the PANI loading increases.

The variation of T_g from decrease to increase can be considered as a criterion to identify the percolation threshold in epoxy resin.[68] Epoxy resin blended with carbon nanotubes (CNTs) and polypyrrole (PPy) has been studied by Barrau et al.[68] The content of filler near the percolation threshold was first obtained by the dc conductivity, and a minimum T_g studied by DSC and dynamic mechanical thermal analysis (DMTA) tests and change of storage modulus were shown in the same range of loading for the percolation threshold to take place. A relationship between the electrical percolation and the T_g variation is built. A similar minimum T_g and variation tendency are observed as the nanofiller loading was increased. Specifically, the T_g value first decreases, and, after reaching the lowest point, it begins to increase as the nanofiller loading increases. It is worth noting that the minimum T_g value is shown at different loadings for the PNCs with nanofibers (3.0 wt %) and nanospheres (5.0 wt %). This variation is associated with morphology difference between the nanofibers and the nanospheres. For the PANI nanofibers with a larger aspect ratio, it would be easy to form a network than the PANI nanospheres in the matrix resin.[26]

3.5. Thermogravimetric Analysis of Cured Epoxy Resin and its Nanocomposites. Figure 6B shows the TGA curves of the cured pure epoxy and its PNCs with two different PANI nanostructures in nitrogen. For all the samples, there is only one sharp weight loss stage, which is caused by the chain breakdown of the polymer structure. From the onset decomposition temperature (extrapolated onset temperature is obtained by software and the temperature range is set to 200−400 °C) summarized in Table 2, the introduction of the PANI nanofillers in the epoxy resin causes the decomposition temperature decrease, which is attributed to the lower decomposition temperature of pure PANI nanofibers (235.15 °C) and PANI nanospheres (251.73 °C) than that of pure epoxy. Similarly, because of the higher decomposition temperature of the pure PANI nanospheres than that of the PANI nanofibers (Figure 1A), the PNCs with nanospheres exhibit an higher onset decomposition temperature than that of the PNCs with nanofibers at the same filler loading (Table 2).

However, when the test was run in air (Figure 6C), different from the results obtained in a nitrogen environment, two weight loss stages are observed. The first degradation stage in air is almost the same as that in the nitrogen case, which is associated with the breaking of the cross-linked network in epoxy and the release of moisture and organic solvent residue entangled in the PANI polymer chains. However, the second

Table 2. Onset Temperature, Weight Loss at 800 °C in Nitrogen, and Glass Transition Temperature of the Cured Pure Epoxy and PNCs with PANI Nanofibers and Nanospheres

sample name	onset temperature (°C)	weight loss (%)	T_g (°C)
cured pure epoxy	375.28	88.02	108.31
PNCs with 1.0 wt % PANI nanofibers	358.63	88.25	94.32
PNCs with 3.0 wt % PANI nanofibers	347.75	87.59	83.83
PNCs with 5.0 wt % PANI nanofibers	339.10	86.58	91.44
PNCs with 10.0 wt % PANI nanofibers	309.49	84.92	95.65
PNCs with 1.0 wt % PANI nanoshperes	365.84	88.79	93.81
PNCs with 3.0 wt % PANI nanospheres	358.85	89.11	89.62
PNCs with 5.0 wt % PANI nanospheres	352.87	86.33	87.73
PNCs with 10.0 wt % PANI nanospheres	337.86	80.86	95.98

stage stems from the structure conversion or oxidation of aromatic rings in epoxy.[69] The PNCs show higher onset decomposition temperature than pure epoxy in this stage (Table 3), which is attributed to the enhanced network

Table 3. Onset Temperature in Air for the Cured Pure Epoxy and PNCs with 10.0 wt % Loading of PANI Nanofibers and Nanospheres

sample name	onset temperature (°C)
cured pure epoxy	524.42
PNCs with 10.0 wt % PANI nanofibers	545.69
PNCs with 10.0 wt % PANI nanospheres	568.75

structure in the PNCs.[70] Compared with pure epoxy, the amine groups of PANI formed covalent bondings with epoxy resin, which can postpone the breakdown of the aromatic rings.[42] Overall, compared with pure epoxy resin, the introduction of PANI increases the thermal stability of epoxy in the high-temperature range in air.

3.6. Flame Retardancy Analysis of Cured Epoxy Nanocomposites. The flame retardancy behaviors of the cured PNCs with different PANI nanostructures were evaluated by studying the heat release (HR) capacity, peak heat release rate (pHRR), total heat release, and char residue, which are summarized in Table 1. (The detailed results of the PNCs with different loading levels of the PANI nanospheres are shown in Table S1 in the Supporting Information.) From the curve of heat release rate (HRR) as a function of temperature (Figure 7), the pHRR, HR capacity, and total HR of the PNCs decrease as the loading of PANI nanofibers increases, which indicates that the existence of PANI nanofillers reduced the heat release from the epoxy resin. Based on the discussion in TGA part, the amine groups of PANI can form covalent bondings with epoxy matrix, which can postpone the breakdown of aromatic rings;[42] thus, the decreased HRR should be associated with the interfacial reaction between PANI and epoxy resin. The PANI nanofillers in epoxy resin inhibited the matrix from pyrolysis and caused a reduced HRR. Moreover, because of the larger specific surface area of the PANI nanofibers than that of the PANI nanospheres,[57] more amine groups of PANI nanofibers

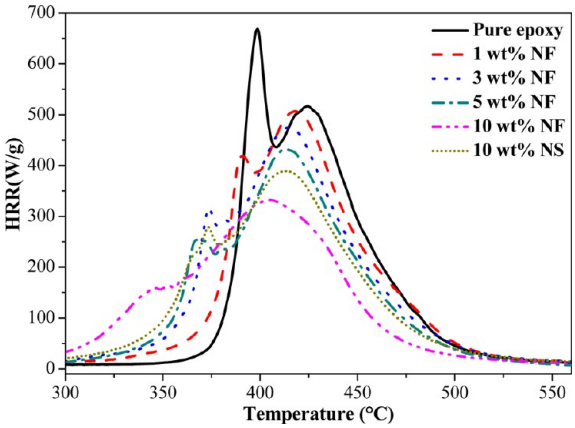

Figure 7. HRR–temperature curves of the cured pure epoxy and its PNCs with PANI nanofibers and nanospheres.

can react with epoxy resin; thus, the interfacial reaction between PANI nanofibers and epoxy resin should be stronger than the reaction between PANI nanospheres and epoxy resin, and, thus, the HRR value of PNCs with the PANI nanofibers is lower than that of the PNCs with the PANI nanospheres. The amine groups of PANI help to reduce the HRR, the nitrogen compound flame retardant has been widely used for flame retardancy with the release of nonflammable gases.[71] It is known that the existence of PANI can help to form carbonaceous components,[72] and the enhanced char residue indicates that the addition of PANI nanofillers favors the char formation of epoxy matrix. Char yield is considered as a denotation of flame retardancy. The formed char on the surface of materials can prevent the heat from being transferred from the heat source to the inner material[73] and also obstruct the distribution of combustible gases produced during the burning process.[74]

3.7. Dynamic Mechanical Properties of Cured Epoxy Resin and Its Nanocomposites. Dynamic mechanical analysis (DMA) shows information of the storage modulus (G'), loss modulus (G''), and tan δ in the test temperature range. The storage modulus represents the elastic property or the energy storage in the nanocomposites, while the loss modulus reflects the viscous behavior or the energy dissipation in the nanocomposites during the test.[75,76] Figure 8A and 8B shows the G' and G'' for the cured pure epoxy resin and its PNCs. In the glass plateau (below 80 °C, when the polymer chains cannot move and the values of both modulii are high), the values of both modulii are almost the same for all the samples. However, when the temperature further increases to the glass-transition range of the samples (80–120 °C, when the polymer segments begin to move and the modulii are sharply decreased), obvious difference is observed among the PNCs with different PANI nanostructures. As the PANI loading increases, G' varies like a wave, i.e., it first decreases and then increases. First, both G' and G'' decrease as the loading of PANI nanofibers increases from 0 to 1.0 wt %; however, when the loading of PANI nanofibers further increases from 1.0 wt % to 3.0 wt %, both G' and G'' increase, and further increase as the loading of PANI nanofibers increases from 3.0 wt % to 5.0 wt %. The lowest value of G' is observed with a PANI nanofiber loading of 1.0 wt %. For the PNCs with nanospheres, G' varies with a similar tendency as that in the PNCs with nanofibers; however, even when the loading is increased to 5.0 wt %, both modulii are still decreased, and the changing point of G' from

dx.doi.org/10.1021/am302563w | ACS Appl. Mater. Interfaces 2013, 5, 898–910

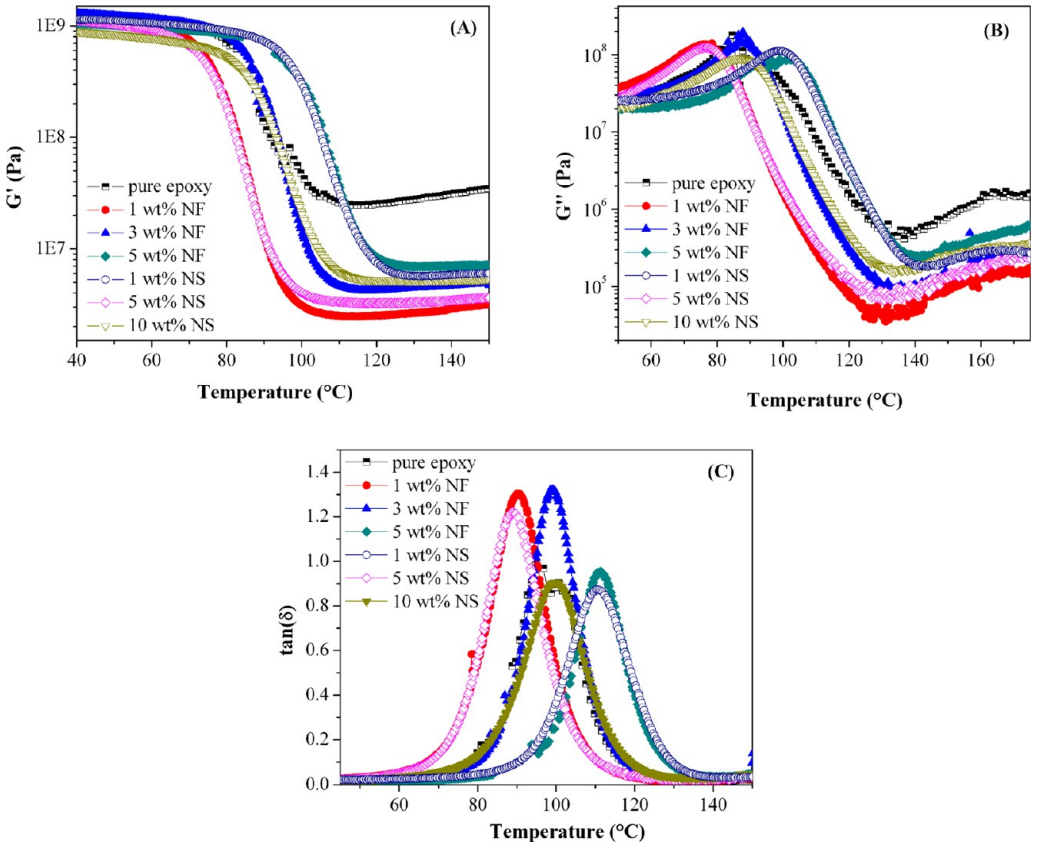

Figure 8. (A) Storage modulus (G'), (B) loss modulus (G''), and (C) tan δ versus temperature of the cured pure epoxy, and its PNCs with different loadings of PANI nanofibers and nanospheres.

decrease to increase occurs when the loading is increased from 5.0 wt % to 10 wt %. The lowest G' value exists with a loading of PANI nanospheres of 5.0 wt %. As formerly mentioned, the variation of G' can also be associated with the percolation threshold for the epoxy nanocomposites; thus, the lowest value of G' can also be considered as a parameter to identify the conductive percolation threshold. Thus, the percolation threshold is 5.0 wt % and 1.0 wt % for nanospheres and nanofibers, respectively. For the PANI nanofibers, the percolation threshold value is slightly lower than that obtained by the T_g value of the DSC test (3.0 wt %).

The tan δ is the ratio of the loss modulus to the storage modulus, and the peak of tan δ is often used to determine the glass-transition temperature (T_g). As shown in Figure 8C, for the PNCs with the PANI nanofibers, T_g first decreases as the loading of PANI nanofibers increases from 0 to 1.0 wt %, which is attributed to the enlarged free volume between the epoxy chains.[67] With further increases in the loading of PANI nanofibers, T_g increases, which is consistent with the result obtained in the modulii part, the lowest value of T_g shown in PNCs with 1.0 wt % PANI nanofibers. For the PNCs with the nanospheres, the lowest value of T_g is shown for 5.0 wt %. The T_g value obtained with the value of tan δ is slightly different from that obtained from the DSC test. To further identify the electrical percolation threshold, the conductive property is further studied.

3.8. Tensile Mechanical Property and Fracture Surface Analysis of Cured Nanocomposites. The breaking tensile stress and modulus of elasticity, each as a function of PANI nanostructure, are shown in Figure 9. The tensile stress of the PNCs decreases as the loading of PANI nanofibers increases;

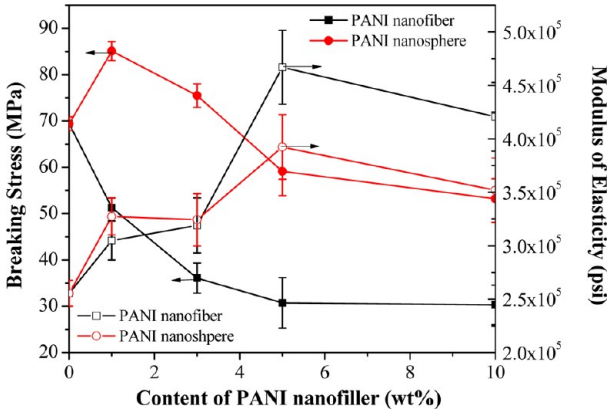

Figure 9. Breaking stress and modulus of elasticity for the cured pure epoxy and the PNCs with different loading levels of PANI nanofibers and nanospheres; the solid and open symbols represent the value of stress and modulus, respectively.

however, for the PNCs with the PANI nanospheres, the stress first increases and then decreases as the loading of nanospheres increases. The fracture surface is observed to be very smooth for pure epoxy, Figure 10, and can be considered as a typical brittle fracture; however, for the epoxy nanocomposites with 1.0 wt % PANI nanospheres, more laminated cracks can be observed on the fracture surface. When the crack is extended from one layer to the other, energy will be absorbed[77] and cause an increased strength in the modulus of elasticity. The increased tensile strength is associated with the covalent bondings between the PANI nanospheres and the hosting

dx.doi.org/10.1021/am302563w | ACS Appl. Mater. Interfaces 2013, 5, 898−910

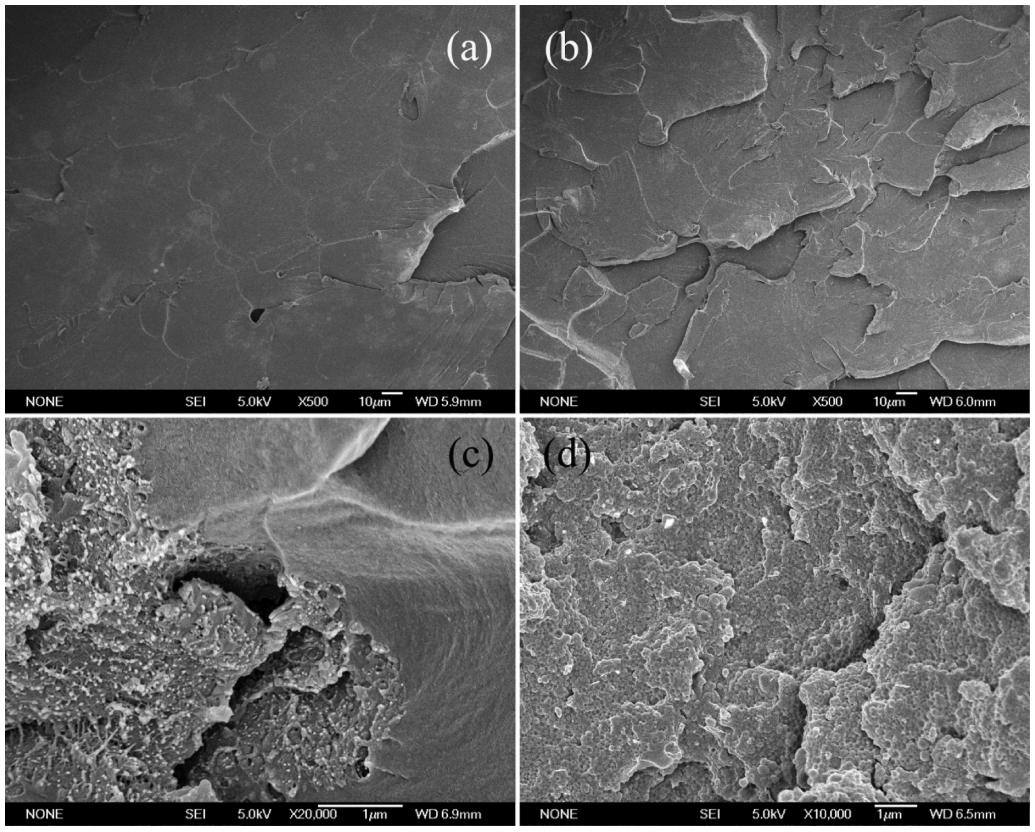

Figure 10. SEM images of the fracture surface of (a) the cured pure epoxy, and the PNCs with (b) 1.0 wt % PANI nanospheres, (c) 10.0 wt % PANI nanofibers, and (d) 10.0 wt % PANI nanospheres, respectively.

epoxy matrix. Although chemical bonding can be formed between the PANI nanofillers and epoxy resin, it is difficult for PANI to be uniformly dispersed; thus, when the loading of PANI nanofillers is increased to 10 wt %, some conductive salt-rich regions can be observed in the fracture surface. On one hand, this indicates the fine network of PANI formed in the matrix;[40,78] on the other hand, it can cause defects and initiate failure,[79] which, in turn, decreases the tensile strength.

Electrical Conductivity (σ) of Cured Nanocomposites. Figure 11 shows the volume resistivity of the PNCs, as a function of the loading of different PANI nanostructures. The resistivity is observed to decrease as the loading of PANI nanostructures increases. However, at the same loading of PANI nanostructures, the volume resistivity of the PNCs with the PANI nanofibers is much lower than that of the PNCs with the PANI nanospheres, and the gap difference between them increases as the loading of PANI nanostructures increases. When the loading increases to 10.0 wt %, the volume resistivity of the PNCs with the PANI nanofibers is even two magnitudes lower than that of the PNCs with the PANI nanospheres. This phenomenon can be associated with the contact resistance[58] and percolation threshold.[36] For the pure PANI nanostructures, the electron transportation follows a three-dimensional (3-D) variable range hopping (VRH) mechanism, and the nanofibers with the highest aspect ratio have the highest conductivity.[58] Before the PANI nanostructures reach the percolation threshold, and with the same loading, the junctions of the PANI nanofibers with a higher aspect ratio are fewer than those in the PANI nanospheres with a lower aspect ratio. Thus, the contact resistivity of the PNCs with the PANI nanofibers is lower than that of the PNCs with the PANI nanospheres. In addition, for the PNCs with the PANI nanofibers, the volume resistivity decreases sharply when the loading of conductive fillers increases from 0 to 3.0 and then the slope of the curve becomes gentle with further increases in the loading. Combined with the discussion in the moduli and T_g, it indicates that the PNCs with the PANI nanofibers have reached the percolation threshold at 3.0 wt %. However, for the PNCs with the PANI nanospheres, the slope changes at a loading of 5.0 wt %. The difference of percolation threshold is associated with the morphology difference of nanofibers and nanospheres. For the PANI nanofibers with a larger aspect ratio, it is easier to reach percolation by forming a network structure than the PANI

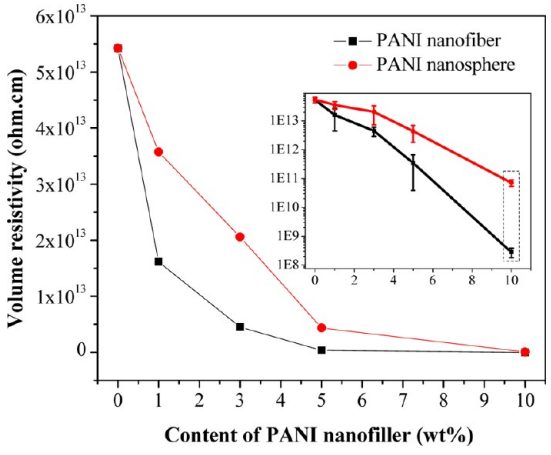

Figure 11. Volume resistivity of the cured pure epoxy and its PNCs with different loading levels of the PANI nanofibers and nanospheres.

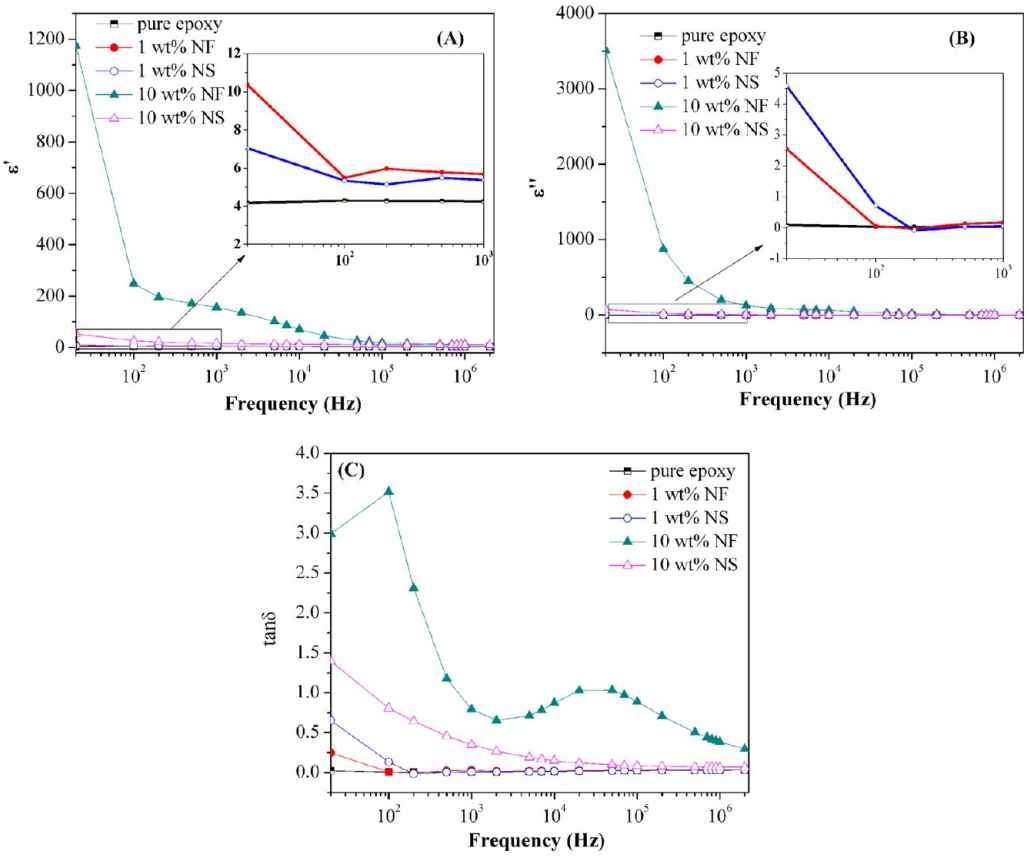

Figure 12. (A) Real permittivity (ε'), (B) imaginary permittivity (ε''), and (C) dielectric loss (tan δ) of the cured pure epoxy and its PNCs with different loading levels of the PANI nanofibers and nanospheres.

nanospheres. As the loading of PANI nanostructures increases, the volume resistivity of the PNCs with the PANI nanofibers decreases more rapidly than that of the PNCs with the PANI nanospheres.

3.10. Dielectric Permittivity. For the dielectric property study, the real permittivity, imaginary permittivity, and dielectric loss are all shown in Figure 12. For all of the samples, both real permittivity and imaginary permittivity decrease with increasing frequency, because of the dipolar groups, which cannot follow the change in the alternative electric field.[80] At lower frequency, the dipolar functional groups can orient themselves and a high permittivity value is observed; however, the dipolar groups cannot orient with the same rate of the alternating electric field at higher frequency and, thus, causes a reduced permittivity.[80] In addition, as the loading of the PANI nanofillers increases, the values of both the real and imaginary permittivity increase and the PNCs with the PANI nanofibers have higher real and imaginary permittivity than the PNCs with the PANI nanospheres. For pure PANI, the value of real permittivity is negative, resulting from the metallic state in PANI;[58] thus, the high positive permittivity in the nanocomposites is not due to the metallic state in PANI and, instead, it is due to the interfacial polarization,[43] which arises from the charge carriers blocked at the internal surface or interfaces between the matrix and the fillers.[81] In the PANI nanofillers, the protons (hydrogen ions) provided by the doping acid can move along the PANI chains; however, these charge movements will be hindered by epoxy resin, resulting in a large number of space charges accumulating at the interface of PANI and epoxy to give a large interfacial polarization. In addition, because of the larger specific surface area of the PANI nanofibers than that of the PANI nanospheres,[57] the interfacial polarization effect between the PANI nanofibers and the hosting epoxy is greater than that between the PANI nanospheres and the epoxy.[82] Thus, the permittivity of the PNCs with the PANI nanofibers is higher than that of the PNCs with the PANI nanospheres. Moreover, for the dielectric loss study (Figure 12C), the observed tan δ of the PNCs, which is much higher than that of pure epoxy, is associated with the free charge motion difference,[40] indicating that an interfacial polarization formed in the PNCs.

4. CONCLUSION

The polymer nanocomposites with different polyaniline (PANI) nanostructures (nanofibers and nanospheres) at different loading levels are prepared and systematically studied. Although the PANI nanostructures caused the onset temperature decrease in nitrogen, it postponed the breakdown of the aromatic rings in air. The flame retardancy studies have successfully demonstrated that the introduction of the PANI nanofillers can decrease the heat release rate of epoxy resin and increase the char residue. Both viscosity and complex viscosity are studied in the rheology test and a reduced viscosity is explained by the shear-thinning behavior of the PNCs. In addition, since the electrical percolation threshold of the epoxy nanocomposites takes place at the minimum value of the moduli and the glass-transition temperature (T_g). The change of G', G'', and tan δ is studied and combined with the results of conductive property. The nanofibers with a higher aspect ratio reach the percolation threshold at a lower loading than the

PANI nanospheres. For the conductivity study, at the same loading level, the observed lower volume resistivity in the epoxy nanocomposites with PANI nanofibers than that in the epoxy nanocomposites with the PANI nanosphere is discussed with the contact resistance difference. The junctions of the PANI nanofibers with higher aspect ratio are fewer than those in the PANI nanospheres with lower aspect ratio; therefore, the resistivity is lower. Both the more-laminated cracks observed from SEM on the fracture surface and the crack extension from one layer to the other causing the energy adsorption contributed to the enhanced modulus of the elasticity. Compared with pure epoxy, the improved dielectric property of the PNCs is attributed to the large interfacial polarization.

■ ASSOCIATED CONTENT

Supporting Information

The molecular structure of Epon 862 and the used curing agent Epicure W, shear stress vs shear rate curves of pure epoxy resin and epoxy resin nanosuspensions with different loadings of PANI nanofibers, DTG curve of the PANI nanofibers and nanospheres, and table for the heat release (HR) capacity, peak heat release rate (pHRR), total heat release, and char residue for the PNCs with PANI nanospheres are given in the supporting materials. This material is available free of charge via the Internet at http://pubs.acs.org.

■ AUTHOR INFORMATION

Corresponding Author

*Tel.: (409) 880 7976 (S.W.), (409) 880-7654 (Z.G.). E-mail: suying.wei@lamar.edu (S.W.), zhanhu.guo@lamar.edu (Z.G.).

Notes

The authors declare no competing financial interest.

■ ACKNOWLEDGMENTS

This project is supported by the National Science Foundation-Nanoscale Interdisciplinary Research Team and Materials Processing and Manufacturing (No. CMMI 10-30755) managed by Dr. Mary Toney. S.W. acknowledges the Welch Foundation (No. V-0004).

■ REFERENCES

(1) Zhu, J.; He, Q.; Luo, Z.; Khasanov, A.; Li, Y.; Sun, L.; Wang, Q.; Wei, S.; Guo, Z. *J. Mater. Chem.* **2012**, *22*, 15928−15938.
(2) He, Q.; Yuan, T.; Zhu, J.; Luo, Z.; Haldolaarachchige, N.; Sun, L.; Khasanov, A.; Li, Y.; Young, D. P.; Wei, S.; Guo, Z. *Polymer* **2012**, *53*, 3642−3652.
(3) Zhu, J.; Wei, S.; Li, Y.; Sun, L.; Haldolaarachchige, N.; Young, D. P.; Southworth, C.; Khasanov, A.; Luo, Z.; Guo, Z. *Macromolecules* **2011**, *44*, 4382−4391.
(4) He, Q.; Yuan, T.; Wei, S.; Haldolaarachchige, N.; Luo, Z.; Young, D. P.; Khasanov, A.; Guo, Z. *Angew. Chem., Int. Ed.* **2012**, *51*, 8842−8845.
(5) Zhu, J.; Wei, S.; Haldolaarachchige, N.; Young, D. P.; Guo, Z. *J. Phys. Chem. C* **2011**, *115*, 15304−15310.
(6) Zhu, J.; Wei, S.; Chen, X.; Karki, A. B.; Rutman, D.; Young, D. P.; Guo, Z. *J. Phys. Chem. C* **2010**, *114*, 8844−8850.
(7) Zhu, J.; Wei, S.; Alexander, M. J.; Dang, T. D.; Ho, T. C.; Guo, Z. *Adv. Funct. Mater.* **2010**, *20*, 3076−3084.
(8) Wei, H.; Yan, X.; Li, Y.; Wu, S.; Wang, A.; Wei., S.; Guo, Z. *J. Phys. Chem. C* **2012**, *116*, 4500−4510.
(9) Wei, H.; Yan, X.; Li, Y.; Gu, H.; Wu, S.; Ding, K.; Wei, S.; Guo, Z. *J. Phys. Chem. C* **2012**, *116*, 16286−16293.
(10) Zhang, X.; Wei, S.; Haldolaarachchige, N.; Colorado, H. A.; Luo, Z.; Young, D. P.; Guo, Z. *J. Phys. Chem. C* **2012**, *116*, 15731−15740.
(11) Zhu, J.; Wei, S.; Zhang, L.; Mao, Y.; Ryu, J.; Karki, A. B.; Young, D. P.; Guo, Z. *J. Mater. Chem.* **2012**, *21*, 342−348.
(12) Zhu, J.; Zhang, X.; Haldolaarachchige, N.; Wang, Q.; Luo, Z.; Ryu, J.; Young, D. P.; Wei, S.; Guo, Z. *J. Mater. Chem.* **2012**, *22*, 4996−5005.
(13) Zhu, J.; Wei, S.; Ryu, J.; Guo, Z. *J. Phys. Chem. C* **2011**, *115*, 13215−13222.
(14) Fini, M.; Giavaresi, G.; Aldini, N. N.; Torricelli, P.; Botter, R.; Beruto, D.; Giardino, R. *Biomaterials* **2002**, *23*, 4523−4531.
(15) Mišković-Stanković, V. B.; Stanić, M. R.; Dražić, D. M. *Prog. Org. Coat.* **1999**, *36*, 53−63.
(16) Wang, C. S.; Shieh, J. Y. *J. Appl. Polym. Sci.* **1999**, *73*, 353−361.
(17) Zhu, J.; Wei, S.; Yadav, A.; Guo, Z. *Polymer* **2010**, *51*, 2643−2651.
(18) Zhu, J.; Wei, S.; Ryu, J.; Budhathoki, M.; Liang, G.; Guo, Z. *J. Mater. Chem.* **2010**, *20*, 4937−4948.
(19) Li, J.; Gao, Y.; Ma, W.; Liu, L.; Zhang, Z.; Niu, Z.; Ren, Y.; Zhang, X.; Zeng, Q.; Dong, H.; Zhao, D.; Cai, L.; Zhou, W.; Xie, S. *Nanoscale* **2011**, *3*, 3731−3736.
(20) Zhu, J.; Wei, S.; Ryu, J.; Sun, L.; Luo, Z.; Guo, Z. *ACS Appl. Mater. Interfaces* **2010**, *2*, 2100−2107.
(21) Mamunya, Y. P.; Davydenko, V. V.; Pissis, P.; Lebedev, E. V. *Eur. Polym. J.* **2002**, *38*, 1887−1897.
(22) Kupke, M.; Wentzel, H. P.; Schulte, K. *Mater. Res. Innovations* **1998**, *2*, 164−169.
(23) Zabihi, O.; Khodabandeh, A.; Mostafavi, S. M. *Polym. Degrad. Stab.* **2012**, *97*, 3−13.
(24) Hendricks, T. R.; Lu, J.; Drzal, L. T.; Lee, I. *Adv. Mater.* **2008**, *20*, 2008−2012.
(25) Jagannathan, S.; Liu, T.; Kumar, S. *Compos. Sci. Technol.* **2010**, *70*, 593−598.
(26) Sandler, J. K. W.; Kirk, J. E.; Kinloch, I. A.; Shaffer, M. S. P.; Windle, A. H. *Polymer* **2003**, *44*, 5893−5899.
(27) Zhu, J.; Kim, J.; Peng, H.; Margrave, J. L.; Khabashesku, V. N.; Barrera, E. V. *Nano Lett.* **2003**, *3*, 1107−1113.
(28) Moon, H. S.; Park, J. K. *Synth. Met.* **1998**, *92*, 223−228.
(29) Tarver, J.; Yoo, J. E.; Dennes, T. J.; Schwartz, J.; Loo, Y. L. *Chem. Mater.* **2008**, *21*, 280−286.
(30) Yoo, J. E.; Cross, J. L.; Bucholz, T. L.; Lee, K. S.; Espe, M. P.; Loo, Y. L. *J. Mater. Chem.* **2007**, *17*, 1268−1275.
(31) Zhu, J.; Gu, H.; Luo, Z.; Haldolaarachige, N.; Young, D. P.; Wei, S.; Guo, Z. *Langmuir* **2012**, *28*, 10246−10255.
(32) Gu, H.; Huang, Y.; Zhang, X.; Wang, Q.; Zhu, J.; Shao, L.; Haldolaarachchige, N.; Young, D. P.; Wei, S.; Guo, Z. *Polymer* **2012**, *53*, 801−809.
(33) Zhu, J.; Wei, S.; Zhang, L.; Mao, Y.; Ryu, J.; Haldolaarachige, N.; Young, D. P.; Guo, Z. *J. Mater. Chem.* **2011**, *21*, 16239−16246.
(34) Yang, S. M.; Chen, J. T. *Synth. Met.* **1995**, *69*, 153−154.
(35) Conklin, J. A.; Huang, S. C.; Huang, S. M.; Wen, T.; Kaner, R. B. *Macromolecules* **1995**, *28*, 6522−6527.
(36) Virji, S.; Huang, J.; Kaner, R. B.; Weiller, B. H. *Nano Lett.* **2004**, *4*, 491−496.
(37) Jia, W.; Tchoudakov, R.; Segal, E.; Joseph, R.; Narkis, M.; Siegmann, A. *Synth. Met.* **2003**, *132*, 269−278.
(38) Belaabed, B.; Wojkiewicz, J. L.; Lamouri, S.; El Kamchi, N.; Redon, N. *Polym. Adv. Technol.* **2012**, *23*, 1194−1201.
(39) Jadhav, R. S.; Patil, K. J.; Hundiwale, D. G.; Mahulikar, P. P. *Polym. Adv. Technol.* **2011**, *22*, 1620−1627.
(40) Lu, J.; Moon, K. S.; Kim, B. K.; Wong, C. P. *Polymer* **2007**, *48*, 1510−1516.
(41) Yang, X.; Zhao, T.; Yu, Y.; Wei, Y. *Synth. Met.* **2004**, *142*, 57−61.
(42) Jang, J.; Bae, J.; Lee, K. *Polymer* **2005**, *46*, 3677−3684.
(43) Liu, C. D.; Lee, S. N.; Ho, C. H.; Han, J. L.; Hsieh, K. H. *J. Phys. Chem. C* **2008**, *112*, 15956−15960.
(44) Ge, C.; Yang, X.; Hou, B. *J. Coat. Technol. Res.* **2012**, *9*, 59−69.
(45) Zhang, X.; Guo, F.; Chen, J.; Wang, G.; Liu, H. *Polym. Degrad. Stab.* **2005**, *87*, 411−418.
(46) Chen, W.; Qu, B. *Chem. Mater.* **2003**, *15*, 3208−3213.

(47) Zhang, S.; Horrocks, A. R.; Hull, R.; Kandola, B. K. *Polym. Degrad. Stab.* **2006**, *91*, 719−725.
(48) Hu, Y.; Wang, S.; Ling, Z.; Zhuang, Y.; Chen, Z.; Fan, W. *Macromol. Mater. Eng.* **2003**, *288*, 272−276.
(49) Sun, Q.; Schork, F. J.; Deng, Y. *Compos. Sci. Technol.* **2007**, *67*, 1823−1829.
(50) Lertwimolnun, W.; Vergnes, B. *Polymer* **2005**, *46*, 3462−3471.
(51) Lu, S. Y.; Hamerton, I. *Prog. Polym. Sci.* **2002**, *27*, 1661−1712.
(52) Banks, M.; Ebdon, J. R.; Johnson, M. *Polymer* **1994**, *35*, 3470−3473.
(53) Laoutid, F.; Bonnaud, L.; Alexandre, M.; Lopez Cuesta, J. M.; Dubois, P. *Mater. Sci. Eng., R.* **2009**, *63*, 100−125.
(54) Kiliaris, P.; Papaspyrides, C. D. *Prog. Polym. Sci.* **2002**, *35*, 902−958.
(55) Jeng, R. J.; Shau, S. M.; Lin, J. J.; Su, W. C.; Chiu, Y. S. *Eur. Polym. J.* **2002**, *38*, 683−693.
(56) Trchová, M.; Matějka, P.; Brodinová, J.; Kalendová, A.; Prokeš, J.; Prokeš, J. *Polym. Degrad. Stab.* **2006**, *91*, 114−121.
(57) Zhu, J.; Chen, M.; Qu, H.; Zhang, X.; Wei, H.; Luo, Z.; Colorado, H. A.; Wei, S.; Guo, Z. *Polymer* **2012**, *53*, 5953−5964.
(58) Zhang, X.; Zhu, J.; Haldolaarachchige, N.; Ryu, J.; Young, D. P.; Wei, S.; Guo, Z. *Polymer* **2012**, *53*, 2109−2120.
(59) Chan, C. K.; Whitehouse, C.; Gao, P.; Chai, C. K. *Polymer* **2001**, *42*, 7847−7856.
(60) Seddon, K. R.; Stark, A.; Torres, M.-J. In *Clean Solvents: Alternative Media for Chemical Reactions and Processing*; Abraham, M. A., Moens, L., Eds.; ACS Symposium Series 819; American Chemical Society: Washington, DC, 2002; pp 34−49.
(61) Venkatraman, S.; Okano, M. *Polym. Eng. Sci.* **1990**, *30*, 308−131.
(62) Wen, Y. H.; Lin, H. C.; Li, C. H.; Hua, C. C. *Polymer* **2004**, *45*, 8551−8559.
(63) Dick, H. B.; Krummenauer, F.; Augustin, A. J.; Pakula, T.; Pfeiffer, N. *J. Cataract Refractive Surg.* **2001**, *27*, 320−326.
(64) Cross, M. M. *J. Colloid Interface Sci.* **1965**, *20*, 417−437.
(65) Zhang, Y.; Xu, J.; Chen, Z.; Qin, C.; Dou, Y. *Polym. Int.* **2007**, *56*, 914−918.
(66) Wisanrakkit, G.; Gillham, J. K.; Enns, J. B. *J. Appl. Polym. Sci.* **1990**, *41*, 1895−1912.
(67) Sun, Y.; Zhang, Z.; Moon, K.-S.; Wong, C. P. *J. Polym. Sci., Part B: Polym. Phys.* **2004**, *42*, 3849−3858.
(68) Barrau, S.; Demont, P.; Maraval, C.; Bernes, A.; Lacabanne, C. *Macromol. Rapid Commun.* **2005**, *26*, 390−394.
(69) Liu, Y.; Du, Z.; Zhang, C.; Li, H. *Int. J. Polym. Anal. Charact.* **2006**, *11*, 299−315.
(70) Radhakrishnan, S.; Sonawane, N.; Siju, C. R. *Prog. Org. Coat.* **2009**, *64*, 383−386.
(71) Horacek, H.; Grabner, R. *Polym. Degrad. Stab.* **1996**, *54*, 205−215.
(72) Stejskal, J.; Trchová, M.; Brodinová, J.; Sapurina, I. *J. Appl. Polym. Sci.* **2007**, *103*, 24−30.
(73) Gilman, J. W. *Appl. Clay Sci.* **1999**, *15*, 31−49.
(74) Liu, Y. L. *Polymer* **2001**, *42*, 3445−3454.
(75) Zhu, J.; Wei, S.; Ryu, J.; Budhathoki, M.; Liang, G.; Guo, Z. *J. Mater. Chem.* **2010**, *20*, 4937−4948.
(76) Fabry, B.; Maksym, G. N.; Butler, J. P.; Glogauer, M.; Navajas, D.; Fredberg, J. J. *Phys. Rev. Lett.* **2001**, *87*, 148102.
(77) Sharon, E.; Gross, S. P.; Fineberg, J. *Phys. Rev. Lett.* **1996**, *76*, 2117−2120.
(78) Tsotra, P.; Gryshchuk, O.; Friedrich, K. *Macromol. Chem. Phys.* **2005**, *206*, 787−793.
(79) Isik, I.; Yilmazer, U.; Bayram, G. *Polymer* **2003**, *44*, 6371−6377.
(80) Singha, S.; Thomas, M. J. *IEEE Trans. Dielectr. Electr. Insul.* **2008**, *15*, 12−23.
(81) Schönhals, A.; Goering, H.; Costa, F. R.; Wagenknecht, U.; Heinrich, G. *Macromolecules* **2009**, *42*, 4165−4174.
(82) Yin, J. B.; Zhao, X. P. *J. Phys. Chem. B* **2006**, *110*, 12916−12925.